ETH zürich

ETH Library

Secondary frequency control of dual-port grid forming control

Conference Paper

Author(s):
Subotic, Irina; Gross, Dominic

Publication date:
2023

Permanent link:
https://doi.org/10.3929/ethz-b-000619620

Rights / license:
In Copyright - Non-Commercial Use Permitted

Originally published in:
https://doi.org/10.1109/PowerTech55446.2023.10202960

This page was generated automatically upon download from the ETH Zurich Research Collection.
For more information, please consult the Terms of use.

Secondary frequency control of dual-port grid forming control

Irina Subotic
Automatic Control Laboratory
ETH Zürich, Switzerland
subotici@ethz.ch

Dominic Groß
Department of Electrical and Computer Engineering
University of Wisconsin-Madison, USA
dominic.gross@wisc.edu

***Abstract*—Grid-forming converters are widely envisioned to be the cornerstone of future converter-dominated power systems. However, standard grid forming (GFM) control strategies assume a fully controllable source with enough headroom behind the converter and only implicitly address renewable generation limits through the converter limits. This can lead to instabilities on time scales of both primary and secondary frequency control and jeopardize the safe and reliable operation of electric power systems. In this work, we leverage the recently proposed dual-port GFM control that maps power imbalances in the grid to the power generation interfaced by the power converter. We show that this mechanism allows for considering and transparently addressing limits of renewable generation (e.g., solar photovoltaics and wind) in primary and secondary frequency control. We illustrate that renewable generation using dual-port GFM control can directly integrate into prevailing secondary control methods such as automatic generation control (AGC). Moreover, we discuss the limitations of standard AGC when one or more areas of a power system are dominated by renewable generation and propose an anti-windup strategy to address the power generation limits of renewables. Finally, we verify our findings in a time-domain, electromagnetic transient (EMT) simulation.**

***Index Terms*—Dual-port grid-forming control, secondary control, renewable generation, power system stability**

I. Introduction

A major transition in the operation of electrical power system is the replacement of the conventional, fuel-based power generation interfaced via synchronous machines by distributed renewable generation interfaced via dc/ac power converters. To ensure reliable and stable grid operation of the system with a significant amount of converter-interfaced renewable generation, primary and secondary control functions of synchronous generators need to be provided through the controls of the dc/ac power converters and curtailed renewable generation and/or energy storage. In contrast to machine-interfaced generation that stabilizes the electrical power systems through a combination of the physical properties (e.g., rotational inertia) and controls (e.g., speed-governor control), today's grid-following converter-interfaced renewable generation is typically controlled to maximize power output and can jeopardize system's reliability and stability [1], [2].

The primary frequency control acts on a timescale of milliseconds to seconds. Control algorithms for a dc/ac power converters can be broadly categorized into i) grid following (GFL) and ii) grid forming (GFM) control. Loosely speaking, GFL control implicitly assumes that the converter's ac terminal is connected to an infinite ac bus providing a well-defined and stable ac voltage waveform and typically controls the voltage at converter's dc terminal to implement maximum power point tracking. However, the ac terminal voltage cannot be treated as an infinite ac bus and standard GFL control using a synchronous reference frame (SRF) phase-locked loop (PLL) may jeopardize system stability [3], [4]. On the other hand, GFM control [5]–[7] imposes a well-defined and stable ac voltage waveform on the grid and provides reliable primary frequency control. However, standard GFM controls proposed in the literature neglect the limits of the converter's power source and may also destabilize the system [8]. In contrast, the recently proposed dual-port GFM control paradigm [9]–[11] does not assume a fully controllable power source behind the converter. Conceptually, the dual-port GFM control maps imbalances in the power system to the power source by mapping ac frequency deviations to dc voltage deviations and thus providing bidirectional grid support [9]–[11].

While primary control arrests frequency deviations on timescales of milliseconds to seconds, the goal of secondary frequency control is to restore the system frequency to its nominal value after an event. The prevailing secondary control approach in transmission systems is so-called automatic generation control that i) returns the system to a stable post-event operating point with nominal frequency, and ii) restores the power exchange between the synchronous inter-areas to their scheduled values. This implicitly rebalances the short term energy (i.e., kinetic energy stored in the machine rotor).

In contrast, in the context of microgrids, different realizations of secondary control methods (e.g., centralized, distributed, decentralized secondary control) have been developed that account for intermittency of renewable generation (e.g., see [12] and references therein). All of those methods rely on microgrid communication infrastructure which introduces scalability challenges. Furthermore, challenges such as clock drifts, cyber-security threats, etc., are also introduced [12]. Finally, secondary control methods for microgrids do not consider power exchange between different synchronous areas and typically do not explicitly account for the power generation interfaced by the power converter [12].

In contrast to previous work on dual-port GFM control, this work investigate integrating renewable generation with GFM control into conventional AGC while explicitly taking into

account the power generation limits of renewables. Conceptually, in bulk-systems, the AGC can update the power set-point of standard GFM controls. However, if the renewable generation interfaced by standard GFM controls does not have sufficient flexibility the system may become unstable on AGC timescales [8]. Therefore, additional energy storage (e.g., batteries), internal energy storage of renewables (e.g., the kinetic energy stored in a wind turbine), and curtailment (i.e., operation below maximal power point) are needed to guarantee safe and stable grid operation on time scales of both primary and secondary frequency control.

In this context, an important feature of the dual-port GFM control is that it maps power imbalances to the power source and makes the internal energy storage of converters [11] and dynamics and inherent energy storage of power generation [9] transparent at the system-level. We leverage these features to account for the limits (e.g., speed limit of the wind turbine (WT), dc voltage limits in a photovoltaic (PV) system, wind turbine pitch motor time constant, etc.) of the converter-interfaced renewable generation. In particular, using energy-balancing dual-port GFM, it becomes clear that the power generation interfaced by a converter needs to be dispatched instead of dispatching the power conversion (i.e., power converter). In this work, we demonstrate that AGC of dual-port GFM control replaces standard AGC functions of conventional synchronous machine-interfaced generation. Moreover, due to their intermittent nature, the converter-interfaced renewable generation might not have enough headroom to respond to power imbalances within their synchronous area. In this case, the AGC has to account for the fact that generation within the synchronous area may reach its power limits. In that case, continuing to integrate the area control error (ACE) will result in integrator windup. Consequently, when the generation is no longer limited, the system may take a very long time to return to its nominal operating point and, during this time, may be vulnerable to disturbances. To overcome this obstacle, we implement an anti-windup strategy that only requires aggregate information about the limits of renewable generation in each area. The proposed control provides a standard secondary control response when sufficient reserves are available and ensures stability when the converter-interfaced renewable generation reaches its limits. Finally, we validate and demonstrate our findings using time-domain EMT simulation.

II. Modeling

In this section, we introduce our model of power conversion elements and renewable generation.

A. Power conversion

We model i) mechanical to electrical conversion via synchronous machines and ii) electrical to electrical conversion via two-level voltage source converters (2L-VSC).

1) Synchronous machine: We use the standard, reduced-order swing equation model given by

$$\tfrac{\mathrm{d}}{\mathrm{d}t}\theta_{r,l} = \omega_{r,l}, \quad J_l\omega_{r,l}\tfrac{\mathrm{d}}{\mathrm{d}t}\omega_{r,l} = P_{\mathrm{g},l} - P_{\mathrm{sm},l}, \tag{1}$$

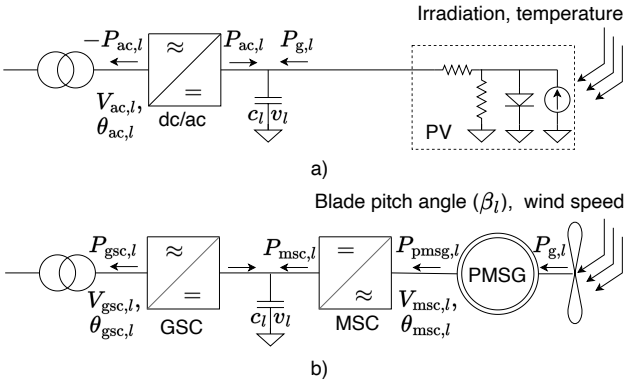

Fig. 1. a) PV system with dc/ac power converter and PV modeled via its equivalent electrical circuit, b) PMSG wind turbine with back-to-back converter connection.

where $\omega_{r,l} \in \mathbb{R}$ and $P_{\mathrm{g},l} \in \mathbb{R}$ are machine rotor frequency and mechanical power applied to the machine rotor. The machine inertia is modeled by $J_l \in \mathbb{R}_{>0}$.

2) dc/ac power converter: While our results apply to more complex voltage source converter topologies, such as modular-multilevel converters (see [11]), for brevity of presentation, we consider a lossless, averaged, 2L-VSC with dc-link charge dynamics given by

$$c_l \tfrac{\mathrm{d}}{\mathrm{d}t} v_l = -P_{\mathrm{ac},l} - P_{\mathrm{dc},l}. \tag{2}$$

The dc voltage and capacitance are denoted by $v_l \in \mathbb{R}_{\geq 0}$ and $c_l \in \mathbb{R}_{>0}$, while $P_{\mathrm{ac},l} \in \mathbb{R}$ and $P_{\mathrm{dc},l} \in \mathbb{R}$ denote the ac and dc active power injections. Typically, references for the ac voltage magnitude $V_{\mathrm{ac},l} \in \mathbb{R}_{>0}$ and ac voltage phase angle $\theta_{\mathrm{ac},l} \in \mathbb{R}_{>0}$ are tracked by inner converter controls. While, the reference for the ac voltage magnitude $V_{\mathrm{ac},l}$ is provided by standard Q-V droop control [6], the reference for the ac voltage phase angle $\theta_{\mathrm{ac},l}$ remains as a control input for the dual-port GFM control (see Sec. III-A).

B. Renewable generation

For brevity of the presentation, we model two prevailing renewable generation technologies: i) solar photovoltaics and ii) wind generation (see Sec. III-B for curtailment strategies).

1) Solar photovoltaics: A single-stage solar photovoltaic (PV) system, depicted in Fig. 1 a), consists of a dc/ac power converter and PV modules. The dc/ac power converter modulates the dc capacitor voltage at the PV terminal into an ac voltage waveform (ac voltage magnitude $V_{\mathrm{ac},l}$ and ac voltage phase angle $\theta_{\mathrm{ac},l}$). Moreover, the power output of the PV modules is a non-linear function of the solar irradiation, temperature, and dc voltage at the PV terminal. We use the single-diode equivalent circuit shown in Fig. 1 a) to model PV's power output as a function of the dc voltage (cf. [13]). For a constant temperature of 25°C and different solar irradiation, Fig. 2 a) illustrates the PV's power-dc voltage characteristic. Given the nominal operating point $(v_l^\star, P_{\mathrm{g},l}^\star)$, the linearized PV model is

$$P_{\mathrm{g},l} = P_{\mathrm{g},l}^\star - k_{\mathrm{g},l}(v_l - v_l^\star). \tag{3}$$

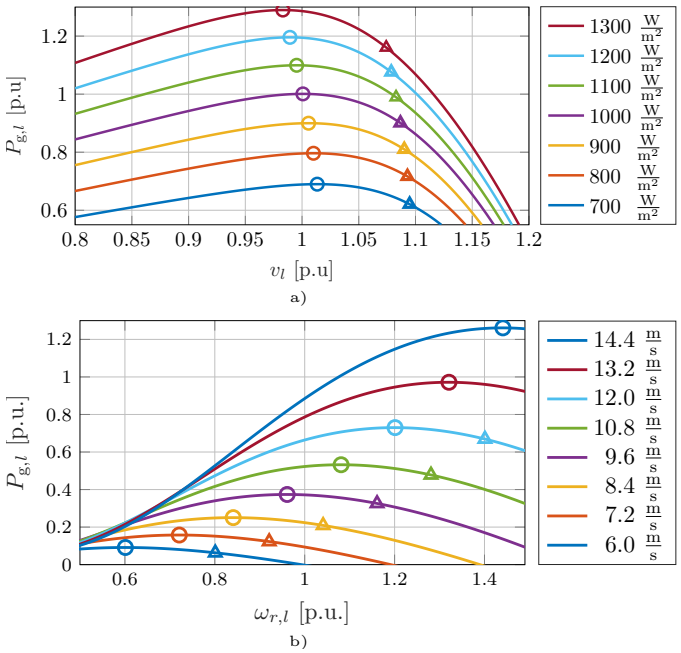

Fig. 2. Steady-state power generation $P_{\mathrm{g},l}$ as a) a function of dc voltage v_l and solar irradiation for PV, and b) a function of rotor speed $\omega_{r,l}$ and wind speed for a WT. Circles denote the MPP, and triangles denote a curtailed operating point (e.g., 90% MPP).

The sensitivity of the PV source is denoted by the constant $k_{\mathrm{g},l} \in \mathbb{R}_{\geq 0}$ which can be obtained by linearizing the PV's power-dc voltage characteristic in Fig. 2 a) around the operating point $(v_l^\star, P_{\mathrm{g},l}^\star)$ (cf. [9]). For a single-stage PV system operated at the maximal power point (MPP), i.e., $v_l^\star = v_l^{\mathrm{MPP}}$, $k_{\mathrm{g},l} = 0$. In contrast, if $v_l^\star > v_l^{\mathrm{MPP}}$ (e.g., triangle in) then, $k_{\mathrm{g},l} > 0$. In other words, when operating the PV system at the MPP, the sensitivity $k_{\mathrm{g},l}$ is zero.

2) Wind power generation: For brevity of the presentation we consider a permanent magnet synchronous generator (PMSG) wind turbine with a back-to-back converter connection, depicted in Fig. 1 b). Conceptually, the PMSG (modeled via (1)) converts the mechanical power generated by the wind turbine $P_{\mathrm{g},l} \in \mathbb{R}_{\geq 0}$ to the electrical $P_{\mathrm{pmsg},l} \in \mathbb{R}_{\geq 0}$. The power flowing out of the PMSG and into the converter is implicitly controlled via machine-side converter (MSC) while the power flowing into the grid is implicitly controlled via grid-side converter (GSC).

The dynamics of a wind turbine are given by (cf. [14])

$$T_{\beta,l}\tfrac{\mathrm{d}}{\mathrm{d}t}\beta_l = -\beta_l + \beta_{u,l}, \;\; P_{\mathrm{g}} = \frac{1}{2}\rho_l \pi R_l^2 C_{p,l}(\lambda_l, \beta_l) v_{\mathrm{w},l}^3, \quad (4)$$

where $\rho_l \in \mathbb{R}_{>0}$ and $R_l \in \mathbb{R}_{>0}$ denote the air density and the rotor radius, while $v_{\mathrm{w},l} \in \mathbb{R}_{>0}$ denotes the wind speed. A function $C_{p,l} : \mathbb{R}_{>0} \times \mathbb{R}_{>0} \to \mathbb{R}_{>0}$ models the fraction of the wind power captured as a function of the blade pitch angle $\beta_l \in \mathbb{R}_{\geq 0}$ and a tip speed ratio $\lambda_l = R_l \omega_{r,l} / v_{\mathrm{w},l}$ where $\omega_{r,l} \in \mathbb{R}_{\geq 0}$ is the PMSG rotor frequency. The blade pitch angle reference is obtained using the controller $\beta_{u,l} := \beta_l^\star + k_{bp,l}(\omega_l - \omega_l^\star)$, with nominal operating point $\beta_l^\star \in \mathbb{R}_{\geq 0}$ and gain $k_{\mathrm{bp},l} \in \mathbb{R}_{\geq 0}$ (cf. [10]). Consequently, the power output of a wind turbine has a non-linear dependence on the wind speed, blade pitch angle and rotor speed. By linearizing the non-linear dynamics (4), around the operating point $(\omega_{r,l}^\star, P_{\mathrm{g},l}^\star)$, we obtain the following dynamics

$$T_{\mathrm{g},l}\tfrac{\mathrm{d}}{\mathrm{d}t}P_{\beta,l} = -(P_{\beta,l} - P_{\beta,l}^\star) - k_{\beta,l}(\beta_l - \beta_l^\star), \quad (5a)$$

$$P_{\mathrm{g},l} = P_{\mathrm{g},l}^\star - k_{\mathrm{g},l}(\omega_l - \omega_l^\star) + P_{\beta,l} - P_{\beta,l^\star}. \quad (5b)$$

The sensitivities of the wind turbine power generation with respect to the rotor frequency and blade pitch angle are denoted by $k_{\mathrm{g},l} \in \mathbb{R}_{\geq 0}$ and $k_{\beta,l} \in \mathbb{R}_{\geq 0}$. While the total generated power is denoted via $P_{\mathrm{g},l} \in \mathbb{R}_{\geq 0}$, $P_{\beta,l} \in \mathbb{R}$ denotes the change in power generation due to changes in blade pitch angle. For zero blade pitch angle, and different wind speeds, the power-machine rotor speed characteristic is illustrated in Fig. 2 b). If $P_{\mathrm{g},l}^\star = P_{\mathrm{g},l}^{\mathrm{MPP}}$, $k_{\mathrm{g},l} = 0$, otherwise $k_{\mathrm{g},l} > 0$. In other words, when operating the wind turbine at the MPP, the sensitivity $k_{\mathrm{g},l}$ is zero.

III. Energy-balancing dual-port GFM control & operating points of renewable generation

In this section, we introduce the energy-balancing dual-port GFM control and discuss strategies to select the operating points of renewable generation.

A. Energy-balancing dual-port GFM control

To obtain the ac voltage phase angle reference, we use the recently proposed energy-balancing dual-port GMF control [9]–[11]

$$\omega_l - \omega_l^\star = k_{d,l}\tfrac{\mathrm{d}}{\mathrm{d}t}(v_l - v_l^\star) + k_{\omega,l}(v_l - v_l^\star). \quad (6)$$

The proportional and derivative feedback gains from the dc voltage deviation to the ac frequency deviation are denoted via $k_{\omega,l} \in \mathbb{R}_{>0}$ and $k_{d,l} \in \mathbb{R}_{>0}$. In principle, the mapping between the dc voltage and ac frequency maps the signals that indicate power imbalances on both terminals of the converter. Hence, by coupling the dc voltage and ac frequency, power imbalances are directly mapped to the power generation interfaced by the converter (cf. [9], [10]). As we will see next, only dc voltage or rotor frequency operating points are needed to rebalance the renewable generation and its inherent internal energy storage.

B. Operating points of renewable generation

The majority of renewable generation deployed today is grid-following and controlled to track the MPP. However, to address variations in the power generation and/or load, with the renewable generation at the MPP a significant amount of energy storage (e.g., battery) is required. Alternatively, the inherent energy storage of renewable generation (e.g., the kinetic energy stored in wind turbines) and curtailment can be used. While medium- and long-term energy storage (e.g., batteries) are needed to provide ancillary services and handle variability on time-scales beyond the secondary control their limited power to energy ratio and degradation due to rapid cycling pose challenges on timescales of primary and secondary control. Therefore, this work investigates how to leverage the inherent energy storage of wind turbines and curtailment

$P^{\star}_{\mathrm{g},l} < P^{\mathrm{MPP}}_{\mathrm{g},l}$, i.e., operation at power generation $P^{\star}_{\mathrm{g},l}$ below the maximal power point (MPP) $P^{\mathrm{MPP}}_{\mathrm{g},l}$. For instance, for PV, $P^{\star}_{\mathrm{g},l}$ is typically chosen between $80\%P^{\mathrm{MPP}}_{\mathrm{g},l}$ and $P^{\mathrm{MPP}}_{\mathrm{g},l}$ [15]. For PV, curtailment can be achieved either by operating a PV system above ($v^{\star}_l > v^{\mathrm{MPP}}_l$) or below ($v^{\star}_l < v^{\mathrm{MPP}}_l$) the dc voltage corresponding to the MPP dc voltage (see Fig. 2 a)) [9]. Similarly, curtailment of a wind generation can be achieved either by operating wind turbine above ($\omega^{\star}_{r,l} > \omega^{\mathrm{MPP}}_{r,l}$) or below ($\omega^{\star}_{r,l} < \omega^{\mathrm{MPP}}_{r,l}$) the rotor speed corresponding to the MPP rotor frequency (see Fig. 2 b)) [9], [10]. Due to the inherent dynamic instability of the operating points below the rotor speed or dc voltage corresponding to the MPP, we focus on curtailment achieved by choosing $v^{\star}_l > v^{\mathrm{MPP}}_l$ and $\omega^{\star}_{r,l} > \omega^{\mathrm{MPP}}_{r,l}$.

1) Single-stage PV: The operating point for the single-stage PV system in Fig. 1 a) is prescribed through the dc voltage set-point $v^{\star}_{\mathrm{dc},l}$. For a curtailed PV system ($v_l > v^{\mathrm{MPP}}_l$), disturbance that occurs in the ac network induces the ac network frequency deviation $\omega_{\delta,l} \coloneqq \omega_l - \omega^{\star}_l$. Dual-port GFM control maps the frequency deviation $\omega_{\delta,l}$ into a dc voltage deviation $v_{\delta,l} \coloneqq v_l - v^{\star}_l$. Moreover, the PV power output responds to the dc voltage deviation $v_{\delta,l}$ according to (3). Consequently, by using dual-port GFM control, if the PV is curtailed, a drop in ac system frequency directly results in an increase in PV power generation according to the power-dc voltage characteristic (see Fig. 2 a)). Thus, the steady-state response of the PV power generation to an ac frequency deviation is given by $P_{\mathrm{g},l} = P^{\star}_{\mathrm{g},l} - \kappa^{-1}_{P,v}\omega_{\delta,l}$, i.e., $\kappa^{-1}_{P,v} \coloneqq k_{\mathrm{g},l}/k_{\omega,l}$ is the frequency control gain (see [9]).

2) Wind generation: While curtailment of wind generation can be achieved through the pitch blade angle and/or through the rotor speed, in this work, we prioritize curtailment through the rotor speed to leverage the significant amounts of kinetic energy that can be stored in the PMSG rotor [10], [16].

In a case of the back-to-back connected wind turbine, as in Fig. 1 b), that is curtailed through the rotor speed ($\omega_{r,l} > \omega^{\mathrm{MPP}}_{r,l}$), we consider GSC and MSC controlled via energy-balancing dual-port GFM. In principle, using the energy-balancing dual-port GFM control on GSC, the ac network frequency deviation $\omega^{\mathrm{gsc}}_{\delta,l} \coloneqq \omega^{\mathrm{gsc}}_l - \omega^{\mathrm{gsc}\star}_{\delta,l}$ is mapped to the dc voltage deviation $v_{\delta,l}$. Next, through the energy-balancing dual-port GFM control on MSC, $v_{\delta,l}$ is mapped to the frequency deviation $\omega^{\mathrm{msc}}_{\delta,l} \coloneqq \omega^{\mathrm{msc}}_l - \omega^{\mathrm{msc}\star}_{\delta,l}$ of the MSC that is identical to the rotor speed deviation $\omega_{r,\delta,l} \coloneqq \omega_{r,l} - \omega^{\star}_{r,l}$. Consequently, the wind turbine power output changes according to the rotor speed deviation $\omega_{r,\delta,l}$ (see Fig. 1 b)). Overall, the steady-state response of a back-to-back connected wind generation to an ac network frequency deviation is given by $P_{\mathrm{g},l} = P^{\star}_{\mathrm{g},l} - \kappa^{-1}_{P,\omega}\omega_{\delta,l}$, i.e., $\kappa^{-1}_{P,\omega} \coloneqq (k^{\mathrm{msc}}_{\omega,l}(k_{\mathrm{g},l} + k_{\beta,l}k_{\mathrm{bp},l}))/k^{\mathrm{gsc}}_{\omega,l}$ is the frequency control gain (see [10]).

3) Renewable generation at the MPP: If renewable generation is operated at MPP (i.e., $v^{\star}_l = v^{\mathrm{MPP}}_l$ and $\omega^{\star}_{r,l} = \omega^{\mathrm{MPP}}_{r,l}$), then $k_{\mathrm{g},l} = 0$. Hence, the frequency control gains $1/\kappa_{P,v} = 1/\kappa_{P,\omega}$ are zero and the renewable generation does not respond to frequency deviations and power imbalances in the ac system. In other words, dual-port GFM control exhibits approximate MPP tracking when $v^{\star}_l = v^{\mathrm{MPP}}_l$ and $\omega^{\star}_{r,l} = \omega^{\mathrm{MPP}}_{r,l}$ (see [9], [10] for further details).

IV. Review of secondary control

For large-scale power systems, the prevailing secondary control mechanism is automatic generation control (AGC). In other words, within each synchronous area, a centralized controller is used to restore frequency to its nominal value $\omega^{\star}$ by redispatching the power generation while accounting for the power exchange $P_{T,i}$ with the neighboring areas. While slightly different realizations of the secondary controller (e.g., integral, proportional-integral) are used in practice, in this work we focus on a centralized proportional-integral controller as detailed in [17]. Using the measurements of the frequency and power exchange with the neighboring areas, the area control error (ACE) for each area i is computed as

$$y_{\mathrm{ACE},i} = P_{T,i} - P^{\star}_{T,i} + B_i(\omega - \omega^{\star}). \tag{7}$$

The scheduled power exchange is $P^{\star}_{T,i} \in \mathbb{R}$ and $B_i \in \mathbb{R}_{>0}$ is the balancing authority bias which it is typically selected to be equal to the aggregate primary frequency control gain of each area. This choice of control gain ensures that the secondary control only responds to the contingencies within its own area. Finally, the standard, centralized PI secondary controller, that computes the incremental power change $P_{s,i} \in \mathbb{R}$ of the power generation dispatch within the area is given by

$$P_{\mathrm{AGC},i} = \beta_i y_{\mathrm{ACE},i} + x_I, \qquad T_{\mathrm{AGC},i}\tfrac{\mathrm{d}}{\mathrm{d}t}x_I = y_{\mathrm{ACE},i}. \tag{8}$$

The power increment $P_{\mathrm{AGC},i}$ is distributed to each unit participating in the secondary control based on its participation factors α_l. In other words, the change in power set-point for the device with index l is $\alpha_l P_{\mathrm{AGC},i}$. To ensure that each control area can be re-balanced for a predefined set of credible contingencies, at present, sufficient secondary control reserves are acquired through market mechanisms.

V. Problem set-up

In contrast to conventional power generation that can be fully dispatched within its rated power, the capabilities of renewable generation depend on environmental conditions such as solar irradiation, temperature, wind speed, etc. We refer to the ability of the converter-interfaced renewable generation to respond to power imbalances in the grid as the flexibility of a renewable generation. The curtailment strategy (see Sec. III-B) and inherent internal storage of the renewable generation are sources of flexibility. In particular, the internal storage of the converter-interfaced power generation is the energy stored in the system (e.g., state-of-charge of a battery, kinetic energy stored in a wind turbine). Nevertheless, limits of the renewable generation have to be taken into account. Renewable generation limits can be broadly categorized into quasi-static and dynamic response limits. The quasi-static limits encompass upper and lower limits on the energy states (e.g., speed limits on a wind turbine, state-of-charge limits on battery, dc voltage limits in a PV system), and maximum (e.g., MPP of PV or wind) and minimum (e.g., back feeding power into a PV module) power generation capability. In contrast,

dynamic response capabilities of the power source include the power generation dynamics and/or response time (e.g., pitch motor time constant of a wind turbine) and additional filters in the control loops of the power generation (e.g., to avoid mechanical damage to a wind turbine).

Apart from the renewable generation limits, the dc/ac power converter is subject to power and current limits. The standard approach in the literature is to attempt to address the quasi-static power generation limits through the dc/ac power converter limits. However, this approach may fail if the quasi-static power limits of the converter-interfaced renewable generation are incorrectly estimated (e.g., MPP of PV) since the converter and renewable generation limits would not be identical [8]. Moreover, addressing power generation limits through the ac/dc power converter limits does not account for the dynamics nor inherent energy storage of the converter-interfaced power generation [15].

Consequently, to overcome this challenge and as a step towards explicitly rebalancing the converter-interfaced renewable generation through secondary control, we leverage the energy-balancing dual-port GFM control (6). The mapping between converter's ac frequency and dc voltage makes the inherent energy storage of the renewable generation (e.g., dc voltage of PV and rotor speed of a WT) transparent to the system and vice-versa. Moreover, if the renewable generation reaches its limit, dual-port GFM control exhibits functions of the standard GFL control without relying on the PLL (see Sec. III-B). Ultimately, converter-interfaced renewable generation can directly be rebalanced through standard secondary control schemes (e.g., AGC) by changing the set-points for the dc voltage (i.e., for a PV) or rotor speed (i.e., for a wind). Hence, the combination of dual-port GFM control and AGC allows for i) systematic coordination of renewable resources and their reserves in a GFM framework, and ii) facilitates their participation in standard secondary frequency control. Moreover, the flexibility and limits of the renewable generation and limits of the dc/ac power converters can be explicitly separated and addressed.

VI. AGC OF DUAL-PORT GFM CONTROLLED RENEWABLE GENERATION AND LEGACY GENERATION

We can use the standard AGC control and update the operating point of the renewable generation according to (8) through the converter dc voltage and frequency set-points. In the remainder of this section, we i) discuss implications of the AGC on the device flexibility, ii) propose an anti-windup enhanced AGC to address stability concerns that arise due to limited energy reserves and flexibility of electrical power systems with significant amount of renewable generation, and iii) discuss the main properties and advantages of AGC of dual-port GFM controlled renewable generation.

A. Renewable generation: set-point update

One of the main advantages of the energy-balancing dual-port GFM control is that it explicitly dispatches the power generation behind the converter through the dc voltage and ac frequency set-points instead of dispatching the power injection of the converter. Hence, the flexibility of a PV can be directly leveraged by changing the dc voltage set-point, while the wind generation is rebalanced by changing the rotor speed set-point. By using the AGC signal $P_{\text{AGC},i}$, computed from (8), for curtailed renewable generation ($k_{\text{g},l} > 0$), we proposed to update the set-points of the converter-interfaced renewable generation using the power generation sensitivities (3),(5) and

$$v^\star_{l,\text{AGC}} = v^\star_l - \frac{\alpha_l}{k_{\text{g},l}} P_{\text{AGC},i},\ \omega^\star_{r,l,\text{AGC}} = \omega^\star_{r,l} - \frac{\alpha_l}{k_{\text{g},l}} P_{\text{AGC},i}. \quad (9)$$

The participation factor is given by $\alpha_l := P^\star_{\text{g},l}/P^\star_\Sigma$, where $P^\star_\Sigma$ is the total power generated in the synchronous area. If $k_{\text{g},l} = 0$, then $\alpha_l = 0$. Therefore, if an area with significant share of the converter-interfaced renewable generation has reserves or flexibility to respond to variations in load or power generation, AGC of dual-port GFM behaves as a standard AGC applied to legacy synchronous generation. However, if system does not have enough reserves, new challenges are introduced.

B. AGC of dual-port GFM: power reserves & anti-windup

In contrast to fully dispatchable synchronous generation, the flexibility of the converter-interfaced renewable generation depends on environmental conditions (e.g., solar irradiation, temperature, wind speed, etc.). Hence, if a synchronous area with significant amount of the converter-interfaced renewable generation participates in the secondary control, its energy reserves and flexibility may be insufficient to cover load variations within the area. This leads to the winding up of the integrator in (8). Consequently, once the load in the synchronous area with insufficient power reserves falls below its generation limits, the system may become unstable. To overcome this obstacle, we use anti-windup feedback, commonly used to limit the integrator output, and modify (8) as follows

$$P_{\text{AGC},i} = \beta_i y_{\text{ACE},i} + x_I, \quad (10a)$$

$$T_{\text{AGC},i} \tfrac{\text{d}}{\text{d}t} x_I = y_{\text{ACE},i} - k_{\text{aw}} \Big(P_{\text{AGC},i} - \text{sat}^{P_{\max,i}}_{P_{\min,i}} (P_{\text{AGC},i}) \Big). \quad (10b)$$

For the setting considered in the manuscript, it suffices to consider the aggregate upper and lower limits $P_{\max,i}$ and $P_{\min,i}$ of the renewable generation in each area at the system-level secondary control. Therefore, assuming large enough areas with diverse renewable generation, it appears reasonable that the aggregate renewable generation limit changes slowly and the limits used in the secondary control layer can be updated on the time scales of markets. A possible approach in addressing limited flexibility of renewable generation is that renewable plant operators only bid control reserves into the secondary control market that the renewable generation can guarantee based on the forecasts and historical data [18]. However, this approach may result in very conservative bids. Rigorously identifying flexibility of the renewable generation and the impact of different bidding strategies is seen as an interesting area for future work. Instead, in this work, we focus on how to avoid instability if all renewable generation within an area reaches its limits.

C. Discussion

If there are enough reserves within the inner-area, AGC of dual-port GFM control behaves as a standard AGC returning the system to the nominal frequency and scheduled inter-area power flows. It also rebalances devices' short-term inherent energy storage without requiring additional coordination. Notably, this approach is fully compatible with prevailing system-level secondary control and device-level control and dynamics of legacy devices (e.g., machine-interfaced generation).

Another advantage of AGC through dual-port GFM control is that the entire range of standard functions of GFL and GFM converters is provided, i.e., from GFM inertia support and primary frequency control to resilient, approximate MPP control without relying on the PLL [9]. Moreover, combination of AGC and dual-port GFM control can be also easily extended to facilitate non-interacting secondary frequency control through high voltage dc transmission [11]. This topic is seen as an interesting area for future research.

Finally, the main control objective of the AGC is returning frequency and the inter-area power flows (tie-line power flows) to their nominal values. However, for areas with a significant amount of converter-interfaced renewables, the necessary power reserves may not be available. Nevertheless, if there are enough reserves in the neighboring areas, the system will stay stable while the frequency and tie-line power flow would not be returned to their nominal values. To improve the situational awareness of AGC, we propose an anti-windup strategy. Moreover, insufficient power reserves can be resolved by i) adding significant storage, or ii) worst-case reserve strategies, but both would require very conservative reserves and likely end up very costly. Alternatively, one could rely on expected values for reserves and only ensure stability but not meet all objectives of secondary frequency control in case there are not enough reserves.

VII. Case Study

Next, we use an EMT simulation to illustrate the results.

A. Benchmark system

We use the IEEE-9 bus system, shown in Fig. 3. The aggregate frequency dynamics of area 1 are modeled through the synchronous generator, at bus 1. Area 2 contains a single-stage PV system (PV, at bus 2) and PMSG wind turbine (WT, at bus 3). The 100MW synchronous generator at bus 1 is modeled using an 8-th order synchronous machine model with AC1A exciter model, automatic voltage regulator, a multi band power system stabilizer, and a first-order turbine model with 5% speed droop. We use 75 MW aggregate model of 5 MW PMSG wind turbines with back-to-back two-level voltage source converters. The PV system parameters are obtained by aggregating 5000 parallel strings of 90 modules (AUO PM060MBR). In other words, the PVs' approximate maximal power and corresponding voltage are 137 MW and 2946 V. Moreover, we use an averaged model of a two-level voltage source converter with RLC filter and cascaded inner current and voltage PI controllers (cf. [19]). The ac lines and dc cables are modeled using the standard π-line dynamics while transformers are explicitly modeled via dynamical models [9].

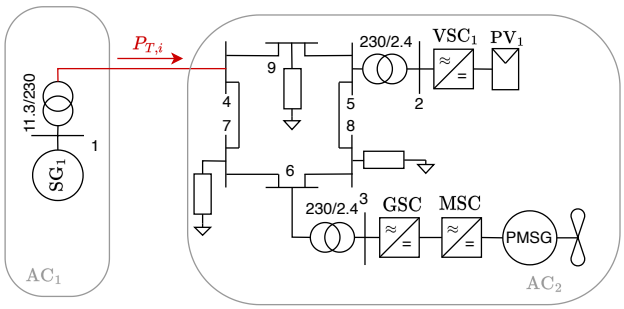

Fig. 3. Benchmark system consist of two ac areas.

Both areas have a nominal frequency of $f_b = 50$ Hz, base power $S_b = 100$ MW, and the nominal ac voltage magnitude is $V_{\text{ac},b} = 230$ kV. The remaining parameters can be found in [9] and references therein.

B. Simulation results

For the nominal operation of the benchmark system described in Sec. VII-A, we simulate i) a sequence with load steps occurring at different times and different locations in the benchmark system, and ii) load steps of different sizes, occurring at the same place in the system for different k_{aw}.

1) Sequence: We simulate the following sequence: i) $t = 1$ min, a load step of 0.075 p.u at bus 8 and bus 1, ii) at $t = 13.75$ min, a load step of 0.1 p.u. at bus 7, and iii) at $t = 21.25$ min, the load step of 0.1 p.u. at bus 7 is removed. The simulation results are shown in Fig 4. We verify the compatibility of the standard AGC and AGC of dual-port GFM control. In particular, after the load steps at $t = 1$ min, each area responds to its own disturbance restoring the frequency to its nominal value and the tie-line power to its scheduled value. Moreover, the operating points of the synchronous generator and renewable generation are updated. After the load step at $t = 13.75$ min, the renewable generation in area 2 reaches its MPP, and area 1 is supplying the remaining power. Consequently, the frequency is not restored to the nominal value and the tie-line power flow deviates from the scheduled. However, due to the anti-windup after the load step is removed at $t = 21.25$ min, the frequency and tie-line power return to their nominal and scheduled values.

2) Different anti-windup gains: To illustrate the influence of the anti-windup on the AGC of dual-port GFM, we simulate i) at $t = 1$ min a load step of 0.2 p.u at bus 8, and remove it ii) at $t \approx 7.2$ min. For different values of the anti-windup gain $k'_{\text{aw}} = k_{\text{aw}}\kappa_{\text{aw}}$, where $\kappa_{\text{aw}} = \{0, 0.2, 0.5, 1, 2, 5, 10\}$, Fig. 5 illustrates the system's behavior after the added load is removed. Standard AGC without anti-windup (i.e., $k'_{\text{aw}} = 0$) does not restore the system to its nominal frequency within a reasonable amount of time and jeopardizes system stability and reliability under subsequent load/generation disturbances. These concerns are resolved by AGC with anti-windup.

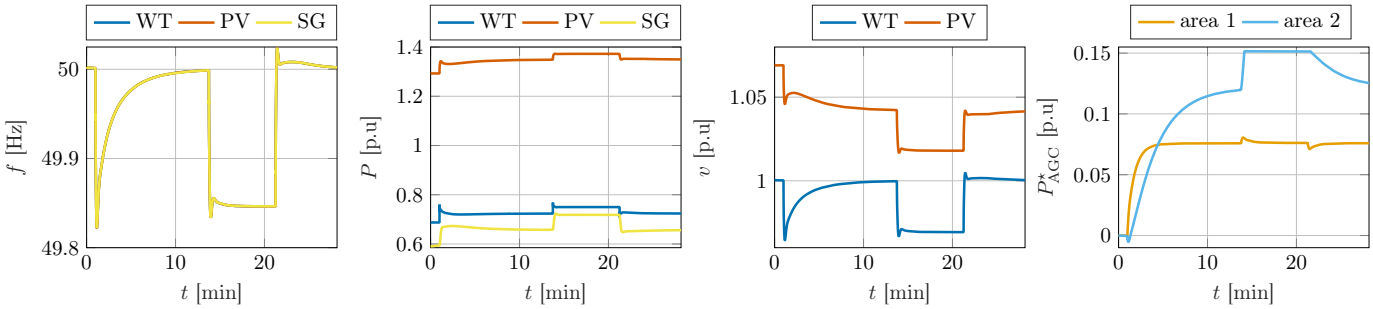

Fig. 4. Simulation results for a series of load steps in area 1 and area 2 of the test system shown in Fig. 3

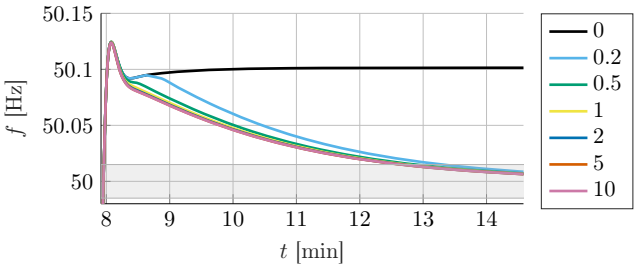

Fig. 5. The frequency response of the test system for different anti-windup gains $k'_{\mathrm{aw}} = k_{\mathrm{aw}}\kappa_{\mathrm{aw}}$ with $\kappa_{\mathrm{aw}} = \{0, 0.2, 0.5, 1, 2, 5, 10\}$. After the added load at bus 8 is removed at $t \approx 7.2$ min the system returns to the nominal frequency range highlighted in gray.

VIII. Conclusion

In this work, we showed that energy-balancing dual-port GFM control is fully compatible with the standard AGC and that it allows to fully leverage the flexibility of renewable generation to facilitate participation in secondary frequency control. In particular, we leveraged reduced-order models to model the limitations of renewables within the context of AGC and developed an anti-windup scheme for AGC in areas dominated by converter-interfaced renewable generation. Finally, the performance of the proposed anti-windup scheme are illustrated and validated using an EMT simulation.

References

[1] W. Winter, K. Elkington, G. Bareux, and J. Kostevc, "Pushing the limits: Europe's new grid: Innovative tools to combat transmission bottlenecks and reduced inertia," *IEEE Power Energy Mag.*, vol. 13, no. 1, pp. 60–74, 2015.

[2] F. Milano, F. Dörfler, G. Hug, D. J. Hill, and G. Verbič, "Foundations and challenges of low-inertia systems (invited paper)," in *Power Systems Computation Conference*, 2018.

[3] "Black system South Australia 28 September 2016," AEMO, Tech. Rep., 2017.

[4] "1,200 MW Fault Induced Solar Photovoltaic Resource Interruption Disturbance Report," NERC, Tech. Rep., 2017.

[5] M. Chandorkar, D. Divan, and R. Adapa, "Control of parallel connected inverters in standalone ac supply systems," *IEEE Trans. Ind. Appl.*, vol. 29, no. 1, pp. 136–143, 1993.

[6] S. D'Arco, J. A. Suul, and O. B. Fosso, "A virtual synchronous machine implementation for distributed control of power converters in smartgrids," *Electr. Pow. Sys. Res.*, vol. 122, pp. 180–197, 2015.

[7] B. Johnson, S. Dhople, A. Hamadeh, and P. Krein, "Synchronization of parallel single-phase inverters with virtual oscillator control," *IEEE Trans. Power Electron.*, vol. 29, no. 11, pp. 6124–6138, 2014.

[8] A. Tayyebi, D. Groß, A. Anta, F. Kupzog, and F. Dörfler, "Frequency stability of synchronous machines and grid-forming power converters," *IEEE Trans. Emerg. Sel. Topics Power Electron.*, vol. 8, no. 2, pp. 1004–1018, 2020.

[9] I. Subotić and D. Groß, "Power-balancing dual-port grid-forming power converter control for renewable integration and hybrid ac/dc power systems," *IEEE Trans. Control. Netw. Syst.*, vol. 9, no. 4, pp. 1949–1961, 2022.

[10] X. Lyu, I. Subotić, and D. Groß, "Unified grid-forming control of PMSG wind turbines for fast frequency response and MPPT," in *Bulk Power System Dynamics and Control Symposium (IREP)*.

[11] D. Groß, E. Sánchez-Sánchez, E. Prieto-Araujo, and O. Bellmunt, "Dual-port grid-forming control of MMCs and its applications to grids of grids," *IEEE Trans. Power Deliv*, vol. 37, no. 6, pp. 4721–4735, 2022.

[12] Y. Khayat, Q. Shafiee, R. Heydari, M. Naderi, T. Dragičević, J. W. Simpson-Porco, F. Dörfler, M. Fathi, F. Blaabjerg, J. M. Guerrero, and H. Bevrani, "On the Secondary Control Architectures of AC Microgrids: An overview," *IEEE Trans. Power Electron.*, vol. 35, no. 6, pp. 6482–6500, 2020.

[13] M. G. Villalva, J. R. Gazoli, and E. R. Filho, "Comprehensive approach to modeling and simulation of photovoltaic arrays," *IEEE Trans. Power Electron.*, vol. 24, no. 5, pp. 1198–1208, 2009.

[14] T. Knudsen and T. Bak, "Simple model for describing and estimating wind turbine dynamic inflow," in *American Control Conference*, 2013, pp. 640–646.

[15] R. H. Lasseter, Z. Chen, and D. Pattabiraman, "Grid-forming inverters: A critical asset for the power grid," *IEEE Trans. Emerg. Sel. Topics Power Electron.*, vol. 8, no. 2, pp. 925–935, 2020.

[16] J. Aho, P. Fleming, and L. Y. Pao, "Active power control of wind turbines for ancillary services: A comparison of pitch and torque control methodologies," pp. 1407–1412, 2016.

[17] "Load-frequency control and performance," UCTE, Tech. Rep., 2004.

[18] C. Konstantinopoulos, I. Avramiotis-Falireas, S. Bolognani, D. Groß, A. Chacko, and G. Hug, "Reliability assessment of pv units in primary and secondary frequency control ancillary services," in *European Energy Market Conference*, 2019.

[19] J. Beerten, S. D'Arco, and J. Suul, "Cable model order reduction for HVDC systems interoperability analysis," in *IET Int. Conf. on AC and DC Power Transmission*, 2015.